UNIVERSITÀ DI PARMA
ARCHIVIO DELLA RICERCA

University of Parma Research Repository

A highly efficient receiver for satellite-based Automatic Identification System signal detection

This is the peer reviewd version of the followng article:

Original
A highly efficient receiver for satellite-based Automatic Identification System signal detection / Colavolpe, G., Foggi, T., Ugolini, A., Lizarraga, J., Cioni, S., Ginesi, A.. - STAMPA. - (2014), pp. 120-127. (2014 7th Advanced Satellite Multimedia Systems Conference and the 13th Signal Processing for Space Communications Workshop (ASMS/SPSC) Livorno (Italy) September 2014) [10.1109/ASMS-SPSC.2014.6934533].

Availability:
This version is available at: 11381/2783187 since: 2015-01-07T20:17:17Z

Publisher:
ESA

Published
DOI:10.1109/ASMS-SPSC.2014.6934533

Terms of use:

Anyone can freely access the full text of works made available as "Open Access". Works made available

Publisher copyright

note finali coverpage

(Article begins on next page)

28 June 2026

A Highly Efficient Receiver for Satellite-Based Automatic Identification System Signal Detection

Giulio Colavolpe*, Tommaso Foggi§, Alessandro Ugolini*, Juan Lizarraga†, Stefano Cioni†, and Alberto Ginesi†
*DII - University of Parma, Viale delle Scienze 181/A, 43124 Parma, Italy, email: giulio@unipr.it
§CNIT, Research Unit of Parma, Viale delle Scienze 181/A, 43124 Parma
†ESA-ESTEC, Noordwijk, The Netherlands

***Abstract*—An innovative receiver architecture for the satellite-based Automatic Identification System (AIS) has been recently proposed. In this paper, we describe a few modifications that can be introduced on the algorithms for synchronization and detection, that provide an impressive performance improvement with respect to the previous system. The receiver architecture has been designed for an on-board implementation, and for this reason all algorithms have been realized keeping the complexity as low as possible. A prototype for the proposed receiver has been implemented by the University of Parma and CGS S.p.A. Compagnia Generale per lo Spazio under the ESA project FENICE.**

I. Introduction

This paper describes an advanced receiver for the reception of Automatic Identification System (AIS) [1] signals from a constellation of Low Earth Orbit (LEO) satellites. A patent application [2] has been filed at the European Patent Office for the receiver described in this paper.

The AIS communication system has been developed to ensure an efficient exchange of information between vessels and shore stations. The exchanged data include information about the identification of each ship, its position, speed, course and other status information. Each station equipped with an AIS transmitter periodically sends short packets that can be received by every AIS receiver within a coverage area of about 40 nautical miles around the transmitter. Each receiver is then able to build a local map of maritime traffic and thus avoid collisions at sea. A system with these characteristics has important ship-monitoring potentialities, with applications to security and search and rescue operations. However, there is a significant limitation caused by the range of coverage: with this system, it is impossible to receive messages from vessels at distances higher than 40 nautical miles from the shore.

For this reason, there has been recently an increasing interest in systems able to receive messages from ships far from the coastline. One way to achieve this goal is to receive messages from a constellation of LEO satellites, ensuring in this way a global coverage. However, the reception of AIS signals from satellites has to face several issues that are not present in terrestrial AIS. In fact, the standard foresees that vessels operating within the same coverage area transmit according to a self-organized time-division multiple access (SOTDMA) protocol, to avoid message collisions. A satellite orbiting with altitudes ranging from 600 to 1000 km has a field of view that can cover multiple SOTDMA cells, so the probability of message collisions increases.

Some works have already addressed the problem of satellite-based AIS reception. For instance, the receiver described in [3] is based on three zonal demodulators processing different (but overlapping) frequency bandwidths (see Fig. 1 for a schematic representation of the three bandwidths), in order to increase the system diversity. The receiver described in this paper has the same architecture as that in [3]; however, we have obtained an impressive performance improvement by replacing the algorithms for synchronization, detection, and post processing with new ones. Throughout the paper, we will compare our proposed receiver with that of [3], and we will highlight the differences and the improvements we have introduced into the system.

As far as the detection algorithm is concerned, another solution has been recently proposed in [4]. In that paper, synchronization aspects are not considered and a full-complexity Viterbi-based decoder, taking into account the characteristics of the modulation and the cyclic redundancy check (CRC) present in the standard, is employed. The authors have also extended this solution to include information on some known bits of the data field in [5]. This solution, while it can be considered as a performance limit, has a huge complexity and is certainly out of reach for an on-board implementation, since the Viterbi decoder operates on a trellis of 2^{18} states. In addition, these receivers have the serious flaw that they will always output a valid codeword, hence loosing the error detection capability typical of CRCs, and the only way to establish whether a message is correct or not would be to actually process the data included in the message itself, compare it with a database of information on previously received packets, and see if the new message is coherent with some previous data. Our aim in this paper is to propose an algorithm that has both a good performance and a complexity that makes it suitable for a practical implementation on board.

The remaining of the paper is organized as follows. Section II describes the signal model considered throughout the paper. Section III details the proposed receiver and Section IV presents some numerical results in terms of packet error rate. Finally, Section V concludes the paper.

978-1-4799-5893-1/14/$31.00 ©2014 IEEE

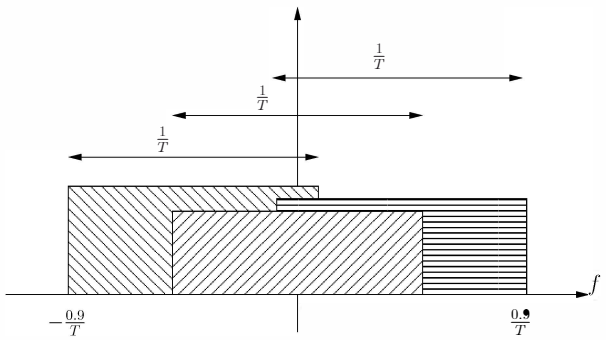

Figure 1. Frequency bandwidths of the three zonal demodulators.

II. System Model and Notation

The complex envelope of a CPM signal can be written as [6]

$$s(t,\boldsymbol{\alpha}) = \sqrt{\frac{2E_S}{T}}\,\exp\left\{j2\pi h\sum_{n=0}^{N-1}\alpha_n q(t-nT)\right\} \quad (1)$$

where E_S is the energy per information symbol, T is the symbol interval, h is the *modulation index*, N is the number of transmitted information symbols, $\boldsymbol{\alpha} = \{\alpha_n\}_{n=0}^{N-1}$ is the information sequence, and $q(t)$ is the *phase pulse*, constrained to be such that

$$q(t) = \begin{cases} 0 & t \le 0 \\ \frac{1}{2} & t \ge LT, \end{cases}$$

L being the *correlation length*. Several examples of commonly used phase pulses are reported in [6].

The modulation index is usually written as $h = r/p$ (where r and p are relatively prime integers), and the information symbols belong to the M-ary alphabet $\{\pm 1, \pm 3, \ldots, \pm(M-1)\}$, M being a power of two. In this case, it can be shown [7] that the CPM signal in the generic time interval $[nT, (n+1)T]$ is completely defined by the symbol α_n, the *correlative state*

$$\omega_n = (\alpha_{n-1}, \alpha_{n-2}, \ldots, \alpha_{n-L+1})$$

and the *phase state* ϕ_n, which can be recursively defined as

$$\phi_n = [\phi_{n-1} + \pi h\alpha_{n-L}]_{2\pi}\ , \quad (2)$$

where $[\cdot]_{2\pi}$ denotes the "modulo 2π" operator. In other words, we may express the complex envelope of a CPM signal as (*Rimoldi decomposition*)

$$s(t,\boldsymbol{\alpha}) = \sqrt{\frac{2E_S}{T}}\sum_{n=0}^{N-1} s_T(t-nT;\alpha_n,\omega_n)e^{j\phi_n}$$

where $s_T(t-nT;\alpha_n,\omega_n)$ is a slice of signal of length T (with support in $[nT,(n+1)T]$) whose shape only depends on symbol α_n and correlative state ω_n and is independent of the considered symbol interval. For the initialization of recursion (2), we adopt the following conventions

$$\begin{aligned} \phi_0 &= 0 \\ \alpha_n &= 0 \quad \forall n < 0\ . \end{aligned}$$

At any given time epoch n, the correlative state ω_n can assume M^{L-1} different values, while the phase state ϕ_n can assume p different values [7], so that the CPM signal can be described by means of a finite-state machine with pM^{L-1} possible values of the state $\sigma_n = (\omega_n, \phi_n)$. When n is even, the p values assumed by the phase state ϕ_n belong to the alphabet $\mathcal{A}_e = \{2\pi hm\,,\ m = 0,1,\ldots,p-1\}$, while, when n is odd, belong to the alphabet $\mathcal{A}_o = \{2\pi hm + \pi h\,,\ m = 0,1,\ldots,p-1\}$.[1] In the remaining parts of the paper, we will adopt the following integer representation for the phase state and information symbols

$$\begin{aligned} \alpha_n &= 2\bar{\alpha}_n - (M-1) \\ \phi_n &= -\pi h(M-1)n + 2\pi h\bar{\phi}_n \end{aligned}$$

so that $\bar{\alpha}_n \in \{0,1,\ldots,M-1\}$ and $\bar{\phi}_n \in \{0,1,\ldots,p-1\}$. The integer $\bar{\phi}_n$ can be recursively updated as follows

$$\bar{\phi}_n = [\bar{\phi}_{n-1} + \bar{\alpha}_n]_p\,.$$

Based on *Laurent decomposition*, the complex envelope of a CPM signal (1) may be exactly expressed as [8]

$$s(t,\boldsymbol{\alpha}) = \sum_{k=0}^{F-1}\sum_{n} a_{k,n}p_k(t-nT) \quad (3)$$

where $F = (M-1)2^{(L-1)\log_2 M}$ is the number of linearly modulated pulses $\{p_k(t)\}$, and $\{a_{k,n}\}$ are the so-called pseudo-symbols (hereafter, simply referred to as symbols). The expressions of pulses $\{p_k(t)\}$ and those of symbols $\{a_{k,n}\}$ as a function of the modulation parameters and of the information symbols $\{\alpha_n\}$ can be found in [8]. By truncating the summation in (3) to the first $K < F$ terms, we obtain the approximation

$$s(t,\boldsymbol{\alpha}) \simeq \sum_{k=0}^{K-1}\sum_{n} a_{k,n}p_k(t-nT)\,. \quad (4)$$

Most of the signal power is concentrated in the first $M-1$ components, i.e., those associated with the pulses $\{p_k(t)\}$ with $0 \le k \le M-2$, which are denoted as *principal components* [8]. As a consequence, a value of $K = M-1$ may be used in (4) to attain a very good tradeoff between approximation quality and number of signal components [9]. A nice feature of the principal components is that their symbols $\{a_{k,n}\}_{k=0}^{M-2}$ can be expressed as a function of α_n and $a_{0,n-1}$ only [8].

The Gaussian minimum shift keying (GMSK) modulation format [10] is a binary CPM (hence, $M = 2$, $\alpha_n \in \{\pm 1\}$, and $E_S = E_b$, where E_b is the energy per information bit) with modulation index $h = 1/2$ and phase pulse mathematically described in [10]. The derivative of this phase pulse can be obtained by filtering a rectangular pulse of length T with a Gaussian filter of proper -3 dB-bandwidth B. In the case of AIS, the value of B normalized to the symbol rate is $BT = 0.4 \div 0.5$. Although in this case the correlation length is in principle unlimited, $L = 2 \div 3$ can be assumed (for our

[1] When r is even, $\mathcal{A}_o$ and $\mathcal{A}_e$ coincide.

simulations we used $L = 3$, but no appreciable difference has been observed with $L = 2$).

Considering now the Laurent representation of a GMSK signal, in this case there is only $M - 1 = 1$ principal component and (4) reads

$$s(t, \boldsymbol{\alpha}) \simeq \sum_n a_{0,n} p_0(t - nT)\,. \tag{5}$$

To simplify the notation, in the following we will use the following definitions:

$$\begin{aligned} a_n &= a_{0,n} \\ p(t) &= p_0(t)\,. \end{aligned}$$

Symbol a_n can be recursively computed as [8]

$$a_n = j\alpha_n a_{n-1}$$

and is related to the phase state ϕ_n by the following equation

$$a_{n-1} = e^{j\phi_n}\,.$$

III. Receiver Structure

The receiver architecture described in this paper has also been considered in [3], and is composed of three zonal demodulators processing different (but overlapping) frequency bandwidths (see Fig. 2 for the block diagram of a zonal demodulator). As described in [3], the signal received from the VHF antenna is first processed by an analog front end and then is subject to an A/D conversion. The resulting discrete-time signal is then properly shifted in frequency and sent to the three zonal demodulators.[2]

Let us now consider a single zonal demodulator. First of all, timing and frequency estimations are performed on the received samples in order to provide the estimates necessary for detection. The estimators work on a window of L_0 symbols and $\eta = 3$ samples per symbol are used. As mentioned, to exploit the frequency diversity given by the Doppler spread, the receiver consists of 3 zonal demodulators, each of which is specifically designed to process only one slice of the AIS channel and to achieve the target performance within that slice. Since the estimation range of the frequency estimator is slightly less than $\pm\frac{0.21}{T}$ and taking into account that, due to a maximum Doppler shift of ± 4 kHz and a maximum frequency uncertainty of transmit and receive oscillators of ± 1.8 kHz, the maximum value of the frequency uncertainty is ± 5.8 kHz$= \pm\frac{0.604}{T}$, it is suggested to center the zonal demodulators at the nominal frequency, at the nominal frequency $+\frac{0.4}{T}$ and at the nominal frequency $-\frac{0.4}{T}$ (see Fig. 1). The next sections will provide a detailed analysis of the components of the zonal demodulator, whose block scheme is represented in Fig. 2.

Each of the three zonal demodulators included in the receiver is composed of four main sub-blocks properly interconnected.

1) *The pre-detection synchronization unit.* This unit performs a preliminary estimation of all channel parameters that need to be compensated before detection. The accuracy of these estimates must be higher than the sensitivity of the detection algorithm to an uncompensated error.
2) *The detection algorithm.*
3) *The post-processing unit.* This unit exploits CRC for frame synchronization and error correction.
4) *The post-detection synchronization unit and the digital re-modulator.* This unit performs a fine estimation of the channel parameters needed for the reconstruction and cancellation of the detected signal. In general, the estimation accuracy must be greater than that of the pre-detection synchronization unit.

In the following sections, we will describe the algorithms employed in these four units.

A. Pre-Detection Synchronization

Aim of this first synchronization stage is to estimate, in a non-data-aided (NDA) mode,[3] and compensate the frequency offset F and the timing offset τ that affect the received signal, whose complex envelope $r(t)$ is modeled by the following equation

$$r(t) = As(t - \tau, \boldsymbol{\alpha}) \exp\{j\theta\} \exp\{j2\pi Ft\} + w(t) \tag{6}$$

where a constant amplitude A, a constant phase offset θ, and a complex additive white Gaussian noise (AWGN) process $w(t)$ with two-sided power spectral density $2N_0$, modeling the noise baseband equivalent, are also accounted for. Note that the interfering users are not included in the model (6), since the interference has been neglected in the receiver design. On the other hand, the impact of the interferers on the receiver performance can be evaluated by means of extensive computer simulations. We also point out that the pre-detection synchronization stage does not attempt to recover the phase offset θ, possibly time-varying, since the selected detection algorithm, described in the next section, can manage the presence of this phase uncertainty (see the relevant description).

The timing and carrier synchronization functions are carried out over a window of only L_0 symbols (bits) of the SOTDMA slot. The reason for this is that the current message alignment is not known at this point, so the synchronization blocks have to be activated on the portion of the slot where transmitted messages would have energy for sure. It turns out that, given the maximum differential delay between messages in the coverage area, only $L_0 = 128$ symbols of the slot can be used when packets of length 224 bits are considered, as those in the AIS 1 and 2 channels. When the shorter packets of length 152 bits, as those in the AIS 3 channels, are considered, it can be assumed $L_0 = 88$.

We empirically found that, in the presence of interference, a performance improvement can be obtained when samples r_n,

[2] Instead of a parallel implementation, to reduce the hardware complexity, the same zonal demodulator can be reused. Obviously, the latency will increase.

[3] Data-aided solutions do not seem to be viable, because of the very low number of known symbols in the transmitted sequence.

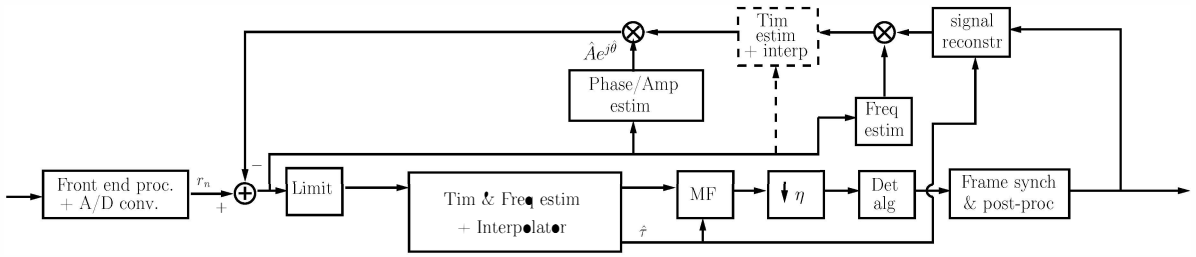

Figure 2. Zonal demodulator.

after cancellation of the previously detected signal, are normalized to unit amplitude. We will say that a *limiter* is applied to the received samples. The advantage of such a transformation in the presence of interference is much higher than the performance degradation resulting in the absence of interference.

Let us now briefly describe the algorithms we have adopted for the pre-detection synchronization stage. The main building block is the synchronization algorithm proposed in [11], and is a modification of that originally selected in [3]. After the limiter, the received samples $\{r_n\}$ are filtered by means of a low-pass filter (LPF), implemented through a finite impulse response (FIR) filter with a limited number of coefficients, having bandwidth B_{LP}, which is a design parameter of the synchronization algorithm. Let $\{z_n\}$ be such filtered samples, indexed from $n = 0$ to $n = \eta L_0 - 1$, which correspond to L_0 signaling intervals. Next, the following coefficients are computed

$$\hat{R}_m(i) = \frac{1}{L_0 - m} \sum_{n=m}^{L_0-1} \left[z_{n\eta+i} z^*_{(n-m)\eta+i} \right]^2$$

for $i \in \{0, 1, \ldots, \eta - 1\}$ and $m \in \{1, 2, \ldots, M_\mathrm{t}\}$, M_t being a design parameter of the synchronization algorithm (we selected a value of $M_\mathrm{t} = 20$). The estimate $\hat{\tau}$ of the time offset is then computed, using only the even autocorrelation terms, as

$$\hat{\tau} = -\frac{T}{2\pi} \arg \left\{ \sum_{i=0}^{\eta-1} \sum_{\substack{m=1 \\ m \text{ even}}}^{M_\mathrm{t}} A_1(m) |\hat{R}_m(i)| \exp\{-j2\pi i/\eta\} \right\} \quad (7)$$

where the terms $\{A_1(m)\}$ are real coefficients that can be precomputed off-line, based only on the modulation format, as explained in [11]. The samples at the limiter output are then interpolated, filtered again, and downsampled, obtaining samples $\{y_n\}$. These latter samples are then employed for frequency estimation by using the algorithm described in [12]. First, the following coefficients are computed

$$R(m) = \frac{1}{L_0 - m} \sum_{n=m}^{L_\bullet - 1} v_n v^*_{n-m}$$

for $m \in \{1, 2, \ldots, M_\mathrm{f}\}$, where M_f is a design parameter not greater than $L_0/2$ (we selected $M_\mathrm{f} = L_0/2$), and $v_n = (-1)^n y_n^2$. Then, the first estimate $\hat{F}_1$ of the frequency offset can be expressed as

$$\hat{F}_1 = \frac{1}{4\pi M_\mathrm{f} T} \sum_{m=1}^{M_\mathrm{f}} w(m) \left[\arg\{R(m)\} - \arg\{R(m-1)\} \right]_{2\pi} \quad (8)$$

where

$$w(m) = \frac{3\left[(L_0 - m)(L_0 - m + 1) - M_\mathrm{f}(L_0 - M_\mathrm{f})\right]}{M_\mathrm{f}(4M_\mathrm{f}^2 - 6M_\mathrm{f}L_0 + 3L_0^2 - 1)}.$$

Finally, a fine frequency estimation is performed by using the algorithm in [11], again adopting only the even autocorrelation terms. Hence, the final estimate $\hat{F}_2$ of the frequency offset is computed as

$$\hat{F}_2 = \frac{1}{4\pi M_\mathrm{t} T} \sum_{\substack{m=1 \\ m \text{ even}}}^{M_\mathrm{t}} \arg \left\{ \mu_m \hat{R}_m(i_m) \hat{R}^*_{m-1}(i_{m-1}) \right\} \quad (9)$$

where the terms $\{\mu_m\}$ are again real coefficients that can be precomputed off-line [11]—for the modulation format of interest here, we obtain $\mu_m = -1$ for all values of m. In (9), $\hat{R}_0(\cdot)$ is conventionally equal to one, while the terms $\{i_m\}$ are computed as explained in [11], or by simply quantizing the value of $\hat{\tau}/T$ to the closest integer (modulo η). The block diagram of the algorithm is shown in Fig. 3.

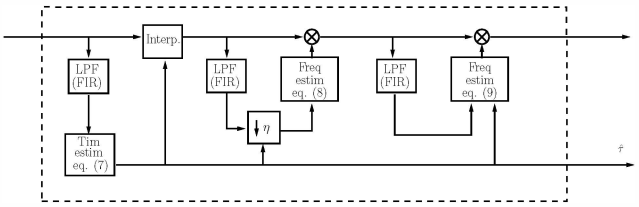

Figure 3. Pre-detection synchronization algorithm.

With respect to the algorithm described in [3], there are some major differences that allow improving the estimation performance. First of all, the original algorithm operates on the samples before the limiter, employs 10 (even and odd) autocorrelation terms instead of 20 (even) terms used now, and finally it performs only one instance of frequency estimation (i.e., the computation of $\hat{F}_1$ is not performed). The use of two instances of frequency estimations is useful to avoid a bias problem of the frequency estimator that reduces the estimation range. On the other hand, the use of the even autocorrelation

terms only and of a different algorithm to compute $\hat{F}_1$, allows to solve a bias problem that appears when a long sequence of zeros in the data field is present (corresponding to particular locations and speeds of the ships).[4]

B. Detection Algorithm

In this section, we detail the detection algorithm employed in the new receiver, that has replaced the Viterbi-based detector in [3]. For the selected detection algorithm, the knowledge of the phase shift introduced by the channel is not necessary, since the detector performs an implicit phase estimation. It is based on the Laurent decomposition (5) and was originally proposed in [13].

The received signal, after frequency and timing estimation and compensation, is filtered by means of an oversampled filter matched to the principal pulse of the Laurent decomposition. One sample per symbol interval is retained at the output of the matched filter (MF) using the information provided by the timing synchronizer. We will denote by x_n the sample at discrete-time n. The channel phase is quantized to the Q values of the alphabet $\Psi = \{0, \frac{2\pi}{Q}, \ldots, \frac{2\pi}{Q}(Q-1)\}$, Q being a design parameter to trade performance against complexity. The channel phase probability density function becomes a probability mass function (PMF) and we will denote by $P_{f,n}(\psi_n)$ and $P_{b,n}(\psi_n)$ the estimates of the channel phase PMF in the forward and backward recursion, respectively. We report here the expression of the forward recursion [13].[5]

$$\begin{aligned} P_{f,n}(\psi_n) =& H_n(\psi_n)\,[(1-P_\Delta)P\{\alpha_n=-1\}P_{f,n-1}(\psi_n) \\ &+ (1-P_\Delta)P\{\alpha_n=1\}P_{f,n-1}(\psi_n+\pi) \\ &+ \frac{P_\Delta}{2}P\{\alpha_n=-1\}P_{f,n-1}\left(\psi_n+\frac{2\pi}{Q}\right) \\ &+ \frac{P_\Delta}{2}P\{\alpha_n=-1\}P_{f,n-1}\left(\psi_n-\frac{2\pi}{Q}\right) \\ &+ \frac{P_\Delta}{2}P\{\alpha_n=1\}P_{f,n-1}\left(\psi_n+\frac{2\pi}{Q}+\pi\right) \\ &+ \frac{P_\Delta}{2}P\{\alpha_n=1\}P_{f,n-1}\left(\psi_n-\frac{2\pi}{Q}+\pi\right)\Big] \end{aligned}$$

where $0 < P_\Delta < 1$ is a design parameter, optimized depending on the speed of variation of the channel phase,[6]

$$H_n(\psi_n) = \exp\left\{\Re\left[\frac{1}{N_0}x_n e^{j\pi h(n+1)}e^{-j\psi_n}\right]\right\} \qquad (10)$$

and $P\{\alpha_n=-1\}$, $P\{\alpha_n=1\}$ are the a-priori probabilities of the symbols. For our simulations, we have set the a-priori probabilities to 0.5, but in a case in which some symbols of the transmitted message are known at the receiver, it is possible to significantly improve the performance of the detection algorithm by including in the detection process the a-priori probabilities of the known symbols. The PMF computed during the forward and backward recursions are employed in the final completion giving the symbol a-posteriori probabilities (APPs):

$$\begin{aligned} P(\alpha_n|\mathbf{x}) = \sum_{\psi_n\in\Psi} & P_{b,n}(\psi_n) \\ & [(1-P_\Delta)P(\bar{\alpha}_n)P_{f,n-1}(\psi_n-\pi\bar{\alpha}_n) \\ & + \frac{P_\Delta}{2}P(\bar{\alpha}_n)P_{f,n-1}\left(\psi_n-\pi\bar{\alpha}_n+\frac{2\pi}{Q}\right) \\ & + \frac{P_\Delta}{2}P(\bar{\alpha}_n)P_{f,n-1}\left(\psi_n-\pi\bar{\alpha}_n-\frac{2\pi}{Q}\right)\Big]. \end{aligned}$$

From the APPs $P(\alpha_n=1|\mathbf{x})$ and $P(\alpha_n=-1|\mathbf{x})$, the logarithmic likelihood ratio (LLR)

$$L_n = \ln\frac{P\{\alpha_n=1|\mathbf{x}\}}{P\{\alpha_n=-1|\mathbf{x}\}}$$

is computed. The receiver takes the following decision on symbol α_n

$$\hat{\alpha}_n = \text{sign}\,[L_n]$$

while $|L_n|$ is an estimate of the reliability of this decision—the larger its value the more reliable the corresponding decision.

The described algorithm is more conveniently implemented in the logarithmic domain [14]. It turns out that, in this case, it is required to compute the logarithm of the sum of exponentials (the Jacobian logarithm), which results to be [14]

$$\begin{aligned} \ln(e^{x_1}+e^{x_2}) &= \max(x_1,x_2)+\ln(1+e^{-|x_1-x_2|}) \\ &\simeq \max(x_1,x_2)\,. \end{aligned}$$

This detection algorithm is a soft-input soft-output (SISO) algorithm. This means that an estimate of the ratio between the signal amplitude and the noise power spectral density N_0 must be available (see eqn. (10)). However, in this case of absence of channel coding this is not critical. On the contrary, the availability of soft decisions represents a powerful tool to improve the receiver performance. In fact, although a channel coding scheme is not adopted in the AIS scenario, we can still use the CRC foreseen by the AIS standard to improve the performance of the adopted SISO detection algorithm, by using the simple post-processing methods described in the next section.

C. Post-Processing Techniques

Frame synchronization based only on the start flag field of the AIS message would be not reliable enough in interference-limited systems as all messages use the same start flag field. Hence, as in [3], the alignment to the start of the message is achieved by using the CRC. In particular, for all 128 possible starting positions of the message, taking into account the maximum differential delay between messages in the coverage area, once a start flag field is observed except for a couple of possible errors, the CRC is verified. When the right position is found, corresponding to a successful verification of the CRC, the decoded message is passed on to the message parser block, which has the functions of discarding duplicated messages

[4]Note that the standard [1] regrettably does not foresee a physical layer scrambling process of the transmitted sequence of symbols.

[5]The backward recursion proceeds similarly.

[6]In the case of a residual frequency error, this parameter has to be optimized accordingly.

and passing the successfully detected messages to the signal reconstruction block of each zonal demodulator. With respect to the approach in [3], we also adopt one of two possible post-processing techniques that can provide an impressive performance improvement. Every time the CRC verification fails, these techniques attempt an error correction. This procedure does not change in the presence of bit stuffing. In fact, in the AIS standard, it is foreseen that if five consecutive ones are found in the bit stream to be transmitted, a zero should be inserted after the five consecutive ones. As a consequence, at the receiver, when five consecutive ones are found followed by a zero, the burst length must be increased by 1 and the initial bit of the CRC field translated accordingly.

Before describing the technique for error correction, we need to explain a property of the AIS modulation format. CPMs are characterized by an intrinsic differential encoding. This means that, at high signal-to-noise ratio (SNR) values, errors occur in couples of consecutive bits. Considering the additional stage of differential encoding foreseen by the AIS standard, the error patterns at high SNR values are in the form "wcw", where "w" represents a wrong bit and "c" a correct one. In addition, at high SNR values, when a packet is wrong, usually a single couple of bit errors occurs. Hence, the two following alternative post-processing stages can be employed.

1) Bit flipping: When the CRC says that the packet is wrong, we assume that only one couple of bits is wrong, so we search for the couple of bits with the lowest reliability and revert them. This operation is performed sequentially on the two least reliable couples by checking every time if a valid codeword (i.e., a codeword satisfying the CRC check) is found after flipping.

2) Syndrome decoding: The syndrome of any valid codeword is always equal to a constant value (it is not zero since the CRC foreseen by the standard is not a linear code due to the particular employed initialization), and the syndrome of an invalid codeword depends only on the error sequence, and is independent of the transmitted sequence. For our purposes, the syndrome corresponds to the CRC of the received sequence. To apply this kind of post-processing, all error patterns containing 1 and 2 couples of wrong bits are tested off-line and the corresponding syndromes are saved into a memory. When receiving a sequence from the detection stage, the following steps are performed:

- the CRC is computed from the received sequence;
- if the computed syndrome equals the syndrome of a correct codeword, the sequence is declared correct;
- otherwise, a search is performed for the computed syndrome among those corresponding to the saved error patterns, starting from those derived from a single couple of errors;
- if a correspondence is found, the word is corrected, otherwise it is declared wrong.

To further improve the reliability of this correction strategy, when searching for errors corresponding to 2 couples of wrong bits, only the couples of bits whose LLRs don't exceed a fixed threshold are corrected (this threshold is a system parameter and, for our simulations, we chose the value of 15).

The second technique outperforms the first one, at the price of an increased computational complexity. An important aspect of both processing techniques is that they maintain the error detection capability of the CRC, since they declare an error if they are unable to correct the received message. In other words, we verified through computer simulations that both techniques negligibly increase the probability that a valid codeword is declared in the presence of errors.

D. Post-Detection Synchronization and Digital Re-Modulation

In this section, we describe the new post-detection synchronization unit and we highlight the differences between this new unit and the one in [3].

When a packet is correctly detected, it can be re-modulated and subtracted from the received signal in order to try to detect other packets. However, the corresponding (time-invariant) amplitude and (time-varying) channel phase, unnecessary to perform detection, must be estimated. In addition, a refined frequency estimate must be also computed since the frequency uncertainty after the pre-detection synchronization stage is larger than that required for a reliable interference cancellation. Through computer simulations, we verified that one of the most critical tasks is represented by the frequency estimation. In fact, in this case a very large accuracy is required. In order to have a limited performance loss with respect to the case of perfect cancellation, the residual frequency error must be lower than $10^{-4}/T$, thus much lower than the frequency error of $10^{-2}/T \div 1.5 \cdot 10^{-2}/T$ tolerated by the described detection algorithm.

Although very efficient data-aided (DA) algorithms based on the *whole* packet are adopted in [3] for frequency, (time-invariant) phase and amplitude estimation, a non negligible performance loss with respect to perfect cancellation is experienced. In order to improve the performance of the estimation algorithms with respect to those proposed in [3], we suggest the following modifications.

First of all, we perform the post-detection synchronization based on the oversampled received signal instead of on the matched filter output. The advantage is that, contrarily to what happens at the output of the matched filter, noise is white and intersymbol interference (ISI) is removed. In other words, it is avoided that ISI and the colored noise degrade the performance. Therefore, we suggest to reconstruct an oversampled version of the detected packet, also necessary to perform cancellation, with time shift provided by the pre-detection stage and arbitrary amplitude and phase. This can be simply done through a discrete-time modulator and an interpolator. Thus, in Fig. 2, the block "signal reconstruction" is, in practice, a discrete-time CPM modulator followed by a quadratic interpolator that, taking into account the timing estimate performed in the predetection stage, tries to align the reconstructed signal and the received samples. Since the discrete-time CPM modulator has to produce 3 samples for each couple (α_n, ϕ_n) (the correlative state is absent in the

978-1-4799-5893-1/14/$31.00 ©2014 IEEE

case of GMSK and the phase state ϕ_n takes on 2 values), it can be conveniently implemented through a look-up table. We will see that, contrarily to what done in [3], it is not necessary to employ the frequency estimate obtained in the pre-detection stage since our post-detection frequency estimator algorithm, that we will now describe, has a sufficiently large estimation range.

Let us denote by $\{\hat{s}_{n\eta+m}\}$ the samples of this reconstructed packet. Frequency estimation is then performed on samples $z_{n\eta+m} = r_{n\eta+m}\hat{s}^*_{n\eta+m}$ by using the DA Mengali and Morelli algorithm [12]. The use of the Mengali and Morelli algorithm, which has the same performance of the Luise and Reggiannini estimator [15] suggested in [3], allows also to remove the main limitation of this latter algorithm. In fact, the Luise and Reggiannini algorithm has an estimation range which depends on the number of symbol intervals observed by the estimator—the larger this number the more limited the estimation range. Considering that the initial frequency uncertainty (after the pre-detection stage) is of $\pm 1.5 \cdot 10^{-2}/T$, the estimator can work by using a very limited number of symbol intervals thus providing a very limited estimation accuracy. To address this problem, in [3] it is suggested to perform frequency synchronization in two steps by using a frequency estimator working on a limited number of symbols in the first step and a second estimator (still based on the Luise and Reggiannini algorithm) working on a larger number of symbols to increase the accuracy. Since the Mengali and Morelli algorithm has an estimation range larger than $\pm 0.2/T$ independently of the number of observed symbol intervals, we can use the whole packet to obtain the most accurate estimate. We verified that, for a given number of observed symbols, the Mengali and Morelli algorithm has the same performance as the Luise and Reggiannini algorithm for both the AWGN scenario and the interference-limited scenario. In addition, they reach the modified Cramer-Rao lower bound (MCRB) in the AWGN scenario. So there is no room for improving the post-detection frequency synchronization. We also verified that there is no performance loss in the frequency estimation when in the presence of the residual timing error before the post-detection frequency synchronization.

Post-detection phase and amplitude estimation can then be performed jointly by using the maximum likelihood (ML) technique. To simplify the notation, we denote by $S_{n\eta+m}$ sample $\hat{s}_{n\eta+m}$ after post-detection frequency estimation and compensation. Denoting by $\hat{\theta}$, and $\hat{A}$, the estimates of phase and amplitude, respectively, the time-varying channel phase is updated using a DA first-order phase-locked loop (PLL) with error signal given by $\Im[r_{n\eta+m}S^*_{n\eta+m}e^{-j\hat{\theta}_{n\eta+m}}]$ whereas the amplitude is estimated as[7]

$$\hat{A} = \frac{\left|\sum_{n=0}^{N-1}\sum_{m=0}^{\eta-1} r_{n\eta+m}S^*_{n\eta+m}e^{-j\hat{\theta}_{n\eta+m}}\right|}{N\eta}$$

[7]To leave out of consideration the initialization of the PLL, a forward and a backward PLL can be employed. The first one is used to estimate the phase in the second half of a packet, whereas the second one will be employed to estimate the phase in the first half packet.

where N is the number of symbol intervals considered for the estimation. Since the complexity is very limited, we have considered estimates based on the whole packet. In our opinion there is no need to use the noncoherent post detection integration suggested in [3] to perform the amplitude estimation since post-detection frequency estimation and compensation has already been performed and an algorithm robust to uncompensated frequency offsets is not required.

It is observed that the cancellation can be improved, thus obtaining a (limited) performance improvement, when timing estimation is refined after post-detection frequency estimation and compensation. We propose to perform this task using the following DA algorithm. First of all, the following quantities are computed:

$$\begin{aligned}
\gamma_0 &= \sum_{n=0}^{N-1}\sum_{m=0}^{\eta-1} r_{n\eta+m}S^*_{n\eta+m}e^{-j\hat{\theta}_{n\eta+m}} \\
\gamma_1 &= \sum_{n=0}^{N-1}\sum_{m=0}^{\eta-1} r_{n\eta+m}S^*_{n\eta+m+1}e^{-j\hat{\theta}_{n\eta+m+1}} \\
\gamma_{-1} &= \sum_{n=0}^{N-1}\sum_{m=0}^{\eta-1} r_{n\eta+m}S^*_{n\eta+m-1}e^{-j\hat{\theta}_{n\eta+m-1}}.
\end{aligned}$$

The refined timing estimate is computed in closed form as

$$\tau = \frac{\eta}{T}\frac{\Re\left[\gamma_0^*\left(\gamma_1 - \gamma_{-1}\right)/2\right]}{\left|\gamma_1 - \gamma_{-1}\right|^2/4 + \Re\left[\gamma_0^*\left(\gamma_1 + \gamma_{-1} - 2\gamma_0\right)\right]}$$

It must be evaluated if this timing refinement and the following quadratic interpolation has a complexity which deserves to be spent considering the limited performance improvement. As can be observed from Fig. 2, the post-detection estimation must be performed using the samples before the limiter.

Finally, we would like to mention the fact that the AIS standard foresees a few symbols of ramp-up and ramp-down at the beginning and at the end of a packet. This must be taken into account during the cancellation, i.e., the reconstructed signal must have appropriate ramp-up and ramp-down intervals. From the analysis of real received AIS packets, we were able to observe the power profile corresponding to the ramp-up and ramp-down sections. Hence, it is possible to estimate the parameters of the power profile and reconstruct the waveform combining these estimated profiles with the reconstructed packet based on detected symbols.

IV. Numerical Results

We assess the performance of the proposed receiver and compare it with that in [3]. The performance will be shown in terms of packet error rate (PER) versus E_b/N_0. In Fig. 4, we consider the case of presence of at most a single interferer in addition to the reference signal (which is that with the highest power), with different values of signal-to-interference power ratio (SIR). Both the reference signal and the interferer have a random normalized Doppler frequency uniformly distributed in the interval $[0, 0.22]$. We report the PER values related to the detection of the reference signal without taking into account the possibility to detect the interferer after successful

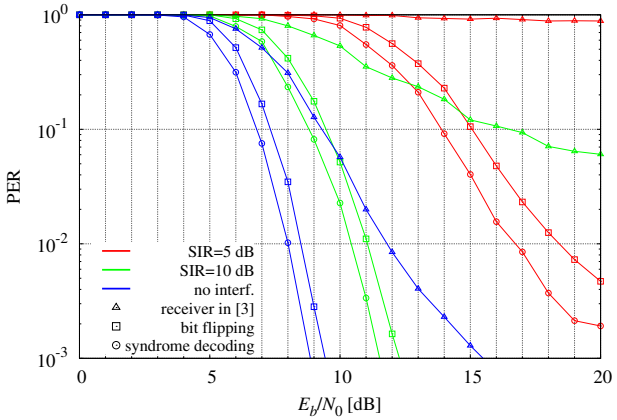

Figure 4. Performance comparison between the proposed receiver and the receiver in [3], for a single interfering signal.

detection and cancellation of the reference signal. Both our proposed post-processing techniques ensure a performance gain of several dBs in both presence and absence of interference from another signal, and the syndrome decoding algorithm gains a further dB with respect to bit flipping. We have performed extensive simulations for other test cases and in worse conditions, like, for instance, in cases when more interfering signals are present. From our results, we have been able to conclude that our receiver has excellent performance, with respect to [3], in all working conditions. However, we have not reported more results in this paper due to a lack of space.

V. Conclusions

This paper proposes several improvements to the receiver described in [3], designed for the reception of AIS signals from LEO satellites. Many of the blocks of [3] have been replaced by more efficient and performing ones. The receiver exhibits excellent performance with respect to [3], and it is suitable for implementations both on board of satellites and in ground-based stations.

VI. Acknowledgements

This work has been conducted by a team under management of CGS S.p.A. and co-funded by the European Space Agency (ESA contract number 4000101838/10/NL/CLP).

References

[1] International Telecommunication Union, "Technical characteristics for an automatic identification system using time division multiple access in the VHF maritime mobile band," *Recommendation ITU-R M.1371-4*, Apr 2010.

[2] G. Colavolpe, T. Foggi, A. Ugolini, J. Lizarraga, S. Cioni, and A. Ginesi, "Receiving method and receiver for satellite-based automatic identification system," Jan. 2014, assigned to ESA-ESTEC, The Neederlands. International patent application n. PCT/EP2014/051273.

[3] P. Burzigotti, A. Ginesi, and G. Colavolpe, "Advanced receiver design for satellite-based automatic identification system signal detection," *International Journal of Satellite Communications and Networking*, vol. 30, pp. 52–63, March/April 2012.

[4] R. Prévost, M. Coulon, D. Bonacci, J. LeMaitre, J.-P. Millerioux, and J.-Y. Tourneret, "CRC-assisted error correction in a trellis coded system with bit stuffing," in *Statistical Signal Processing Workshop (SSP), 2011 IEEE*, June 2011, pp. 381–384.

[5] ——, "Extended constrained Viterbi algorithm for AIS signals received by satellite," in *Satellite Telecommunications (ESTEL), 2012 IEEE First AESS European Conference on*, Oct 2012, pp. 1–6.

[6] J. B. Anderson, T. Aulin, and C.-E. W. Sundberg, *Digital Phase Modulation*. New York: Plenum Press, 1986.

[7] B. E. Rimoldi, "A decomposition approach to CPM," *IEEE Trans. Inform. Theory*, vol. 34, pp. 260–270, Mar. 1988.

[8] U. Mengali and M. Morelli, "Decomposition of M-ary CPM signals into PAM waveforms," *IEEE Trans. Inform. Theory*, vol. 41, pp. 1265–1275, Sep. 1995.

[9] G. Colavolpe and R. Raheli, "Reduced-complexity detection and phase synchronization of CPM signals," *IEEE Trans. Commun.*, vol. 45, pp. 1070–1079, Sep. 1997.

[10] K. Murota and K. Hirade, "GMSK modulation for digital mobile radio telephony," *IEEE Trans. Commun.*, vol. 29, pp. 1044–1050, Jul. 1981.

[11] M. Morelli and U. Mengali, "Joint frequency and timing recovery for MSK-type modulation," *IEEE Trans. Commun.*, vol. 47, pp. 938–946, Jun. 1999.

[12] U. Mengali and M. Morelli, "Data-aided frequency estimation for burst digital transmission," *IEEE Trans. Commun.*, vol. 45, pp. 23–25, Jan. 1997.

[13] A. Barbieri and G. Colavolpe, "Simplified soft-output detection of CPM signals over coherent and phase noise channels," *IEEE Trans. Wireless Commun.*, vol. 6, no. 7, pp. 2486–2496, Jul. 2007.

[14] P. Roberston, E. Villebrun, and P. Hoeher, "Optimal and sub-optimal maximum a posteriori algorithms suitable for turbo decoding," *European Trans. Telecommun.*, vol. 8, no. 2, pp. 119–125, March/April 1997.

[15] M. Luise and R. Reggiannini, "Carrier frequency recovery in all-digital modems for burst-mode transmissions," *IEEE Trans. Commun.*, vol. 43, pp. 1169–1178, Mar. 1995.